# Spin Crossover in Fe(II) and Co(II) Complexes with the Same Click-Derived Tripodal Ligand

David Schweinfurth,[†] Serhiy Demeshko,[‡] Stephan Hohloch,[†] Marc Steinmetz,[§] Jan Gerit Brandenburg,[§] Sebastian Dechert,[‡] Franc Meyer,[‡] Stefan Grimme,*,[§] and Biprajit Sarkar*,[†]

[†]Institut für Chemie und Biochemie, Anorganische Chemie, Fabeckstraße 34-36, D-14195, Berlin, Germany
[‡]Institut für Anorganische Chemie, Georg-August-Universität Göttingen, Tammannstraße 4, D-37077, Göttingen, Germany
[§]Mulliken Center for Theoretical Chemistry, Institut für Physikalische und Theoretische Chemie, Universität Bonn, Beringstraße 4, D-53115, Bonn, Germany

S *Supporting Information*
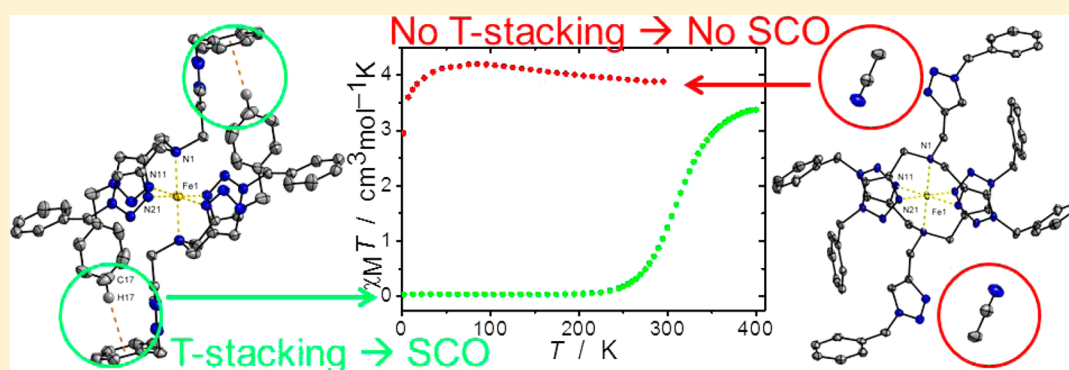
ABSTRACT: The complexes $[Fe(tbta)_2](BF_4)_2 \cdot 2EtOH$ (**1**), $[Fe(tbta)_2](BF_4)_2 \cdot 2CH_3CN$ (**2**), $[Fe(tbta)_2](BF_4)_2 \cdot 2CHCl_3$ (**3**), and $[Fe(tbta)_2](BF_4)_2$ (**4**) were synthesized from the respective metal salts and the click-derived tripodal ligand tris[(1-benzyl-1*H*-1,2,3-triazol-4-yl)methyl]amine (tbta). Structural characterization of these complexes (at 100 or 133 K) revealed Fe−N bond lengths for the solvent containing compounds **1−3** that are typical of a high spin (HS) Fe(II) complex. In contrast, the solvent-free compound **4** show Fe−N bond lengths that are characteristic of a low spin (LS) Fe(II) state. The Fe center in all complexes is bound to two triazole and one amine N atom from each tbta ligand, with the third triazole arm remaining uncoordinated. The benzyl substituents of the uncoordinated triazole arms and the triazole rings engage in strong intermolecular and intramolecular noncovalent interactions. These interactions are missing in the solvent containing molecules **1**, **2**, and **3**, where the solvent molecules occupy positions that hinder these noncovalent interactions. The solvent-free complex (**4**) displays spin crossover (SCO) with a spin transition temperature $T_{1/2}$ near room temperature, as revealed by superconducting quantum interference device (SQUID) magnetometric and Mössbauer spectroscopic measurements. The complexes **1**, **2**, and **3** remain HS throughout the investigated temperature range. Different torsion angles at the metal centers, which are influenced by the noncovalent interactions, are likely responsible for the differences in the magnetic behavior of these complexes. The corresponding solvent-free Co(II) complex (**6**) is also LS at lower temperatures and displays SCO with a temperature $T_{1/2}$ near room temperature. Theoretical calculations at molecular and periodic DFT-D3 levels for **1−4** qualitatively reproduce the experimental findings, and corroborate the importance of intermolecular and intramolecular noncovalent interactions for the magnetic properties of these complexes. The present work thus represents rare examples of SCO complexes where the use of identical ligand sets produces SCO in Fe(II) as well as Co(II) complexes.

■ INTRODUCTION

Octahedral metal complexes with a $d^4−d^7$ electronic configuration can, in principle, exist in the high spin (HS) or low spin (LS) states.[1] The stabilization of one spin state or the other is dependent on the interplay between the ligand field stabilization energy (LFSE) and the spin pairing energy. Magnetic bistability is observed for systems where these two energy terms are comparable in magnitude, and such systems can be switched between the two spin states by using external perturbations such as temperature; this is a phenomenon that is known as spin crossover (SCO).[2−4] Octahedral Fe(II) complexes[3] and Co(II) complexes[5] are the ones that have been investigated the most, with respect to their SCO properties. In this context, it is well-established that ligands with different ligand field strengths are required for generating SCO behavior in Fe(II) and Co(II) complexes. SCO compounds have fascinated both physicists and chemists over

the past decades, because of, on the one hand, the intriguing fundamental physics and chemistry underlying such systems, and, on the other hand, their proposed application in future electronic devices.[6]

Targeted ligand modification has been the most common approach adopted by chemists to tune the spin state of a metal complex. Thus, our knowledge of the types of ligands that might stabilize either an HS or LS state at a metal center is quite advanced, and, hence, our predictive power in that direction has reached a satisfactory level.[1] The same ligand design approach is also essentially at the heart of generating SCO complexes.[2] However, the fine-tuning of a set of either intramolecular or intermolecular covalent or other noncovalent interactions, that are usually responsible for driving SCO in metal complexes, remains a highly challenging and difficult task.[3f] Recently, some examples have appeared in the literature where such noncovalent interactions (NCIs) and their effect on the magnetic properties of the complexes have been investigated in detail.[3f,7] Hence, even though various examples are known of metal complexes that display SCO, the specific interactions which are responsible for making SCO happen, as well as cooperativity effects in the crystal lattice, remain, at best, difficult to understand and, in the worst case, impossible to decipher.[3f] As a result of this, targeted modifications of covalent or noncovalent interactions (crystal engineering) that might either make or break the SCO phenomenon in a particular system remains a field where much still needs to be done and understood.

We have recently reported on a complex $[Co(tbta)_2](ClO_4)_2$ (**5**), where tbta is the click-derived tripodal ligand tris[(1-benzyl-1H-1,2,3-triazol-4-yl)methyl]amine (see Scheme 1).[8]

Scheme 1. Ligand tbta
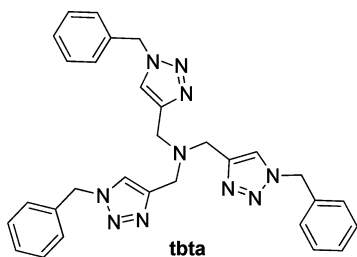
Click-derived triazole ligands have become extremely popular in coordination chemistry, because of a set of extraordinary properties that they impart on their metal complexes.[9−11] Complex **5** displays SCO near room temperature, and it was shown for **5** that certain intermolecular and intramolecular weak, noncovalent interactions are responsible for driving SCO in that complex.[8] For **5**, evidence for the importance of weak, noncovalent interactions was indirect, as this was proved by the example of two other Co(II) complexes that contain tris[(1-cyclohexyl-1H-1,2,3-triazol-4-yl)methyl]amine and tris[(1-n-butyl-1H-1,2,3-triazol-4-yl)methyl]amine, respectively, as ligands. These complexes do not show the aforementioned noncovalent interactions, and they remain HS throughout the entire investigated temperature range.[8] It can be argued that changing substituents on the ligand backbone might intrinsically modify ligand field strength of a ligand, thus making the HS state stable and preventing SCO. In trying to decipher the importance of these interaction for SCO in metal complexes, we turned our attention to some Fe(II) analogues of **5**. Our

aim in turning to the Fe(II) complexes was to modify these noncovalent interactions in a set of complexes containing tbta as the only ligand, thus avoiding any direct modification of the ligand backbone. Furthermore, we wanted to check if SCO observed in the Co(II) complex **5** can be seen in a corresponding Fe(II) complex with the same ligand set. In the following, we present the synthesis, characterization, and structural analyses of $[Fe(tbta)_2](BF_4)_2 \cdot 2EtOH$ (**1**), $[Fe(tbta)_2](BF_4)_2 \cdot 2CH_3CN$ (**2**), $[Fe(tbta)_2](BF_4)_2 \cdot 2CHCl_3$ (**3**), and $[Fe(tbta)_2](BF_4)_2$ (**4**). In addition, we also present a new complex $[Co(tbta)_2](BF_4)_2$ (**6**) to show that the SCO behavior is not dependent on the anions for these complexes (the analogous Co(II) complex, **5** has ClO_4^- as the counteranion). The magnetic properties of these complexes and the existence of possible SCO phenomenon in them were probed by superconducting quantum interference device (SQUID) magnetometry and Mössbauer spectroscopy. In addition, we present evidence from theoretical calculations that helps us in deciphering the importance of noncovalent interactions better. It should be noted that examples of solvent-induced structural and magnetic changes in metal complexes do exist in the literature.[12]

■ RESULTS AND DISCUSSION

Synthesis and Structural Characterization. The complexes were prepared by refluxing 1 equiv of $Fe(BF_4)_2 \cdot 6H_2O$ with 2 equiv of tbta and the subsequent crystallization of the solution (see the Experimental Section). For **6**, the same procedure was applied by using $Co(BF_4)_2 \cdot 6H_2O$ as the metal precursor. The final isolation of crystalline material, and their structural and magnetic properties, turned out to be highly dependent on the type of solvents used for crystallizing these substances. Compounds **1**−**3** are colorless solids, whereas **4** is yellow at ambient temperatures. All compounds showed excellent agreements for their C, H and N values in their combustion tests (see the Experimental Section).

The complexes **1**−**3** crystallize in the monoclinic $P2_1/c$ space group with two solvent molecules per molecule of the complex (see Table S1 in the Supporting Information). In each of the complexes, the Fe(II) center is coordinated in an octahedral fashion through two nitrogen donors of two different triazole rings, and an amine nitrogen donor from each tbta ligand (see Figure 1, as well as Figures S1 and S2 in the Supporting Information). One triazole arm from each tbta ligand remains uncoordinated. The Fe−N11 and Fe−N21 distances to the two triazole N donors are 2.120(5) and 2.154(5) Å, respectively, in the case of **1**. The Fe−N1 distance to the central amine for **1** is 2.307(5) Å. For **2** and **3**, the Fe−N11 distances are 2.132(1) and 2.164(2) Å, respectively, and the Fe−N21 distances are 2.135(1) and 2.108(2) Å, respectively. The distance between Fe(II) and the central amine Fe−N1 for **2** and **3** are 2.294(1) and 2.351(2) Å, respectively. All these Fe−N distances point to a HS Fe(II) center for the complexes at the measured temperatures (100 or 133 K).[3f] The distortion parameter (Σ) values,[3f,13] which describes the sum of the deviation of the 12 cis N−Fe−N angles from an ideal 90° in the octahedron, are 128.2°, 136.4°, and 136° for **1**, **2**, and **3**, respectively. Such relatively high values are typical for an octahedrally coordinated HS Fe(II) center where the distortion from an ideal octahedral environment is usually large.[3f]

No significant intramolecular or intermolecular NCI were detected for any of the compounds **1**−**3** containing solvent molecules in the crystal lattice. The ligand tbta is known to
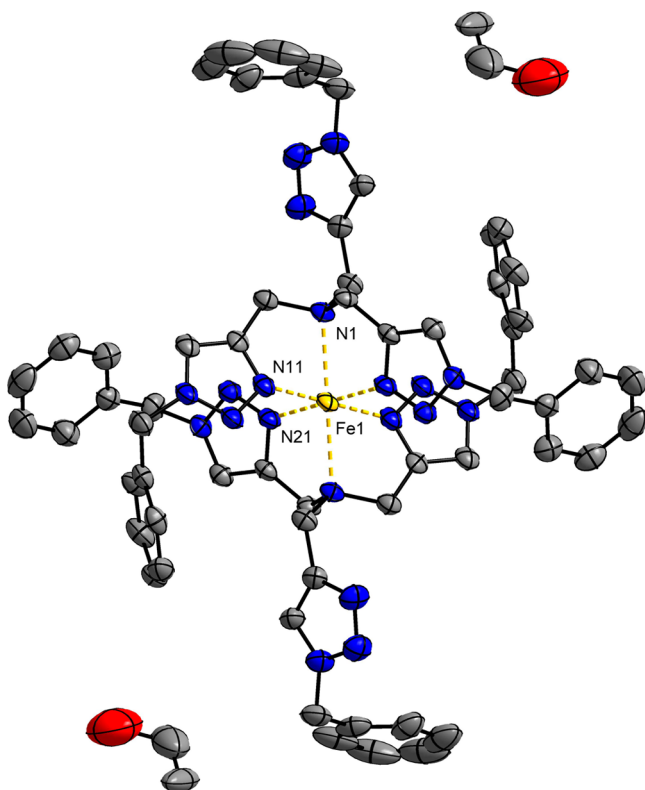
Figure 1. ORTEP plot of **1**. Measurements at 133 K. Ellipsoids are drawn at 50% probability. Hydrogen atoms and counteranions have been omitted for the sake for clarity.

Figure 2. ORTEP plot of **4**. Measurements at 133 K. Ellipsoids are drawn at 50% probability. Hydrogen atoms and counteranions have been omitted for the sake of clarity.

undergo such interactions, as we recently observed in the case of the LS Co(II) complex **5**, as well as other related complexes.[8,11d] In the case of **5**, we had observed strong intramolecular C−H···π interactions between the phenyl rings of the benzyl groups.[8] For **1**−**3**, the solvent molecules included in the crystal lattice seem to disrupt these NCIs and the loss of these intramolecular interactions has a direct impact on the spin state of the molecules. This disruption is best seen in the case of **1**, where the EtOH molecules reside exactly at the position where the intramolecular C−H···π interaction between the phenyl rings would otherwise take place (see Figure 1).

In order to have a direct comparison, we were interested in crystallizing the solvent-free [Fe(tbta)$_2$]$^{2+}$. Gratifyingly, the use of propylene glycol indeed led to the crystallization of the solvent-free Fe(II) complex **4**. Complex **4** crystallizes in the triclinic $P\overline{1}$ space group (see Table S1 in the Supporting Information). The Fe(II) center in **4** is octahedrally coordinated by two triazole and one amine N donor from each tbta ligand (see Figure 2). The Fe−N11 and Fe−N21 distances (Fe−N(triazole)) are 1.948(1) and 1.960(2) Å, respectively. The Fe−N1 (Fe−N(amine)) distance is 2.150(1) Å. The Fe−N distances here are typical of a LS Fe(II) center and, hence, are much shorter than the corresponding distances for **1**−**3**.[3f] The decrease in Fe−N bond lengths upon going from the HS complexes **1**−**3** to the LS complex **4** is ∼0.16 Å for the Fe−N(amine) distances and ∼0.18 Å for the Fe−N(triazole) distances (see Table 1). The distortion parameter Σ has a value of 71.7° for **4**, which is much smaller than those observed for **1**−**3**. The LS Fe(II) center in **4** forms a more regular octahedron than the HS Fe(II) centers in **1**−**3** and this leads to a lower Σ value.[3f,13]
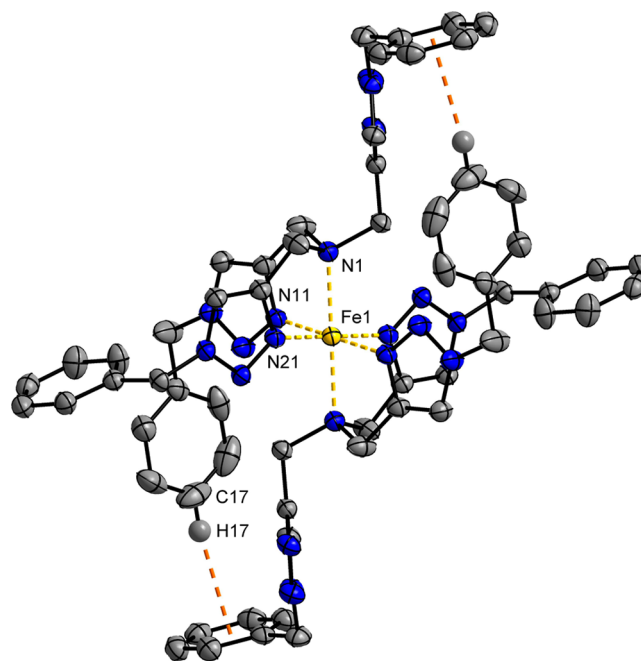
Substituents on the 1,2,3-triazole ring, and the components of the ring itself are known to engage in relatively strong NCI.[14] In **4**, the benzyl rings of the noncoordinating triazole arms of the tbta ligands now participate in various intramolecular and intermolecular NCIs (see Figure 3). The most significant of these are the strong intramolecular C−H···π interactions (see Figures 1, 2, and Supporting Information) between the C−H group of one phenyl ring and the π-system of another phenyl ring. The relevant distance here is 2.688(1) Å. These interactions are disrupted in **1**−**3** by the solvent molecules. The intramolecular and intermolecular NCI seem to force a more compact coordination at the Fe(II) center, thus favoring its LS state. The average of the four (two each) Fe−N11−N12−N13 and Fe−N21−N22−N23 torsion angles in the plane where the triazole rings coordinate to the iron center are 157°, 159°, 157°, and 171° for **1**, **2**, **3**, and **4**, respectively (see Figures 2 and 3). The structure of **4** was also determined at 293 K. The average Fe−N distances in **4** at 293 K are longer than those observed at 133 K (see Table 1 and Figure S3 in the Supporting Information). However, the average of the four torsion angles (see above) at 293 K is 171°; this value is the same as that observed at 133 K for **4**.

The solvent-free Co(II) complex **5** previously reported by us contains ClO$_4^-$ as the counteranion.[8] In order to prove that counterions do not play a role in the spin state determination of these complexes, the Co(II) complex **6** was also crystallized with BF$_4^-$ as counteranion (which is an analogue of **5**). Complex **6** crystallizes in the triclinic $P\overline{1}$ space group (see Table S1 in the Supporting Information). The Co(II) center is bound to the tbta ligand in a similar fashion as that done for **4** and **5** (see Figure 4). The Co−N11 and Co−N21 distances to the two triazole N atoms are 1.919(2) and 1.937(2) Å, respectively. The Co−N1 distance to the central amine N atom is 2.358(2) Å. These distances are typical for a LS Co(II) center.[5] In comparison to the LS Fe(II) complex **4**, the difference between the Co−N(triazole) and Co−N(amine)

Table 1. Bond Lengths of Complexes

	Bond Length (Å)					
	1	2	3	4 (133 K)	4 (293 K)	6
Fe−N1	2.307(5)	2.2940(9)	2.351(2)	2.150(1)	2.191(1)	2.358(2)[a]
Fe−N11	2.120(5)	2.132(1)	2.164(2)	1.948(1)	1.990(2)	1.919(2)[a]
Fe−N21	2.154(5)	2.135(1)	2.108(2)	1.960(2)	2.013(2)	1.937(2)[a]
H17···π				2.6883(3)		2.7598(1)

[a]The distances for **6** refer to Co-donor atom distances.

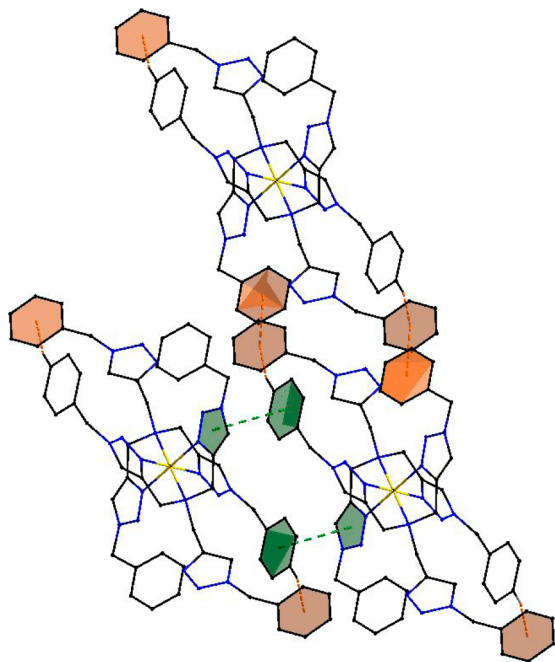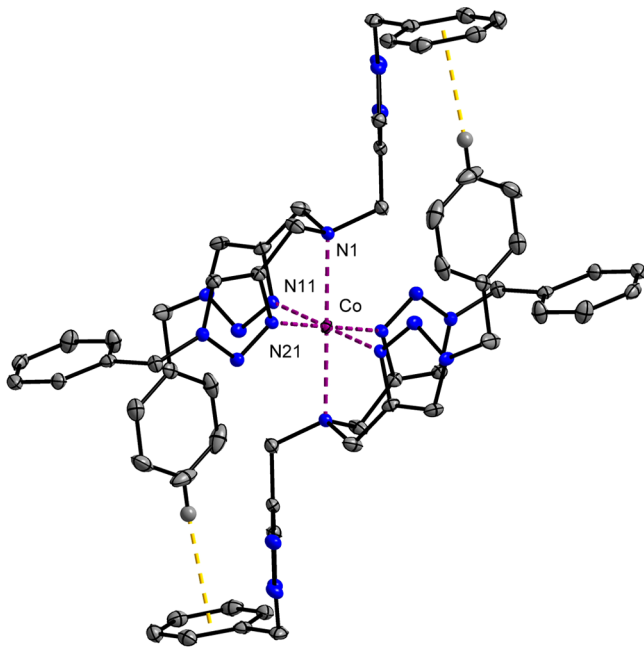**Figure 3.** C−H···π and π··· π interactions in **4**.

Figure 4. ORTEP plot of **6**. Measurements at 100 K. Ellipsoids are drawn at 50% probability. Hydrogen atoms and counteranions have been omitted for the sake of clarity.

distances for **6** are much larger. This is related to the Jahn−Teller distortion observed for the octahedral LS d^7 Co(II) center in **6**.[5,8] The Jahn−Teller distortion leads to substantial elongation of the axial Co−N bonds in **6**. Such an effect is absent in the LS octahendral d^6 Fe(II) center in **4**. The same Jahn−Teller distortion is responsible for a larger Σ value (92.8°) in **6**, compared to that of **4** (71.7°). Just as for **4** and **5**, in complex **6**, the benzyl substituents of the uncoordinated triazole rings of the tbta ligands participate in strong intramolecular and intermolecular C−H···π and π···π interactions. The relevant intramolecular C−H···π distance in this case is 2.759(1) Å. The average of the four (two each) Co−N11−N12−N13 and Co−N21−N22−N23 torsion angles in the plane where the triazole rings coordinate to the Co center is 172° and is comparable to the value observed for **4**.

It should be noted here that all the solvent containing complexes **1**−**3** crystallize in the same monoclinic $P2_1/c$ space group. Similarly, all the solvent free complexes **4**−**6** crystallize in the same triclinic $P\bar{1}$ space group (see Table S1 in the Supporting Information). Thus, the NCI and spin states also seem to be related to a particular crystal system and space group for these complexes.

Magnetic and Spectroscopic Properties. For octahedral Fe(II) complexes, the change in the spin state from $S = 2$ to $S = 0$ upon going from the HS state to the LS state makes them ideal candidates to be probed by SQUID magnetometry.[3] The solvent containing Fe(II) complexes **1**−**3** show $\chi_M T$ values at room temperature in the range of 3.9−4.1 cm³ mol⁻¹ K, which are indicative of HS Fe(II) centers (see Figure S4 in the Supporting Information).[3] No significant changes in the susceptibility values were observed upon cooling the samples to 2 K, indicating that the HS state of the Fe(II) centers is preserved in complexes **1**−**3**, even at lower temperatures (slight deviations of the χT curve from linearity may arise from orbital contributions).

In contrast to complexes **1**−**3**, the solvent-free modification of Fe(II) complex **4** shows a different temperature dependence. The $\chi_M T$ value at 400 K is 3.37 cm³ mol⁻¹ K; however, when the sample is cooled, a SCO phenomenon is observed with a temperature $T_{1/2}$ of 310 K (see Figure 5).

Below 225 K, complex **4** exists in its LS Fe(II) state, as indicated by the $\chi_M T$ values being close to zero. The temperature dependence of the HS molar fraction (γ) could be fitted with the domain SCO model[15] to give the thermodynamic parameters $n·\Delta H$ = 37.2 kJ mol⁻¹ and $n·\Delta S$ = 119 J mol⁻¹ K⁻¹, where n is the domain size and represents the number of molecules per domain. Taking into account that typical ΔS values for Fe(II) SCO complexes lie in the range of 40−65 J mol⁻¹ K⁻¹,[4e,16,17] the n parameter appears to be ∼2 or 3. The substantial domain size is also reflected by the relative abruptness of the SCO conversion curve (Figure 5);[18] the transition is clearly more abrupt than expected for a simple two-state Boltzmann distribution. Thus, it is seen that the SCO
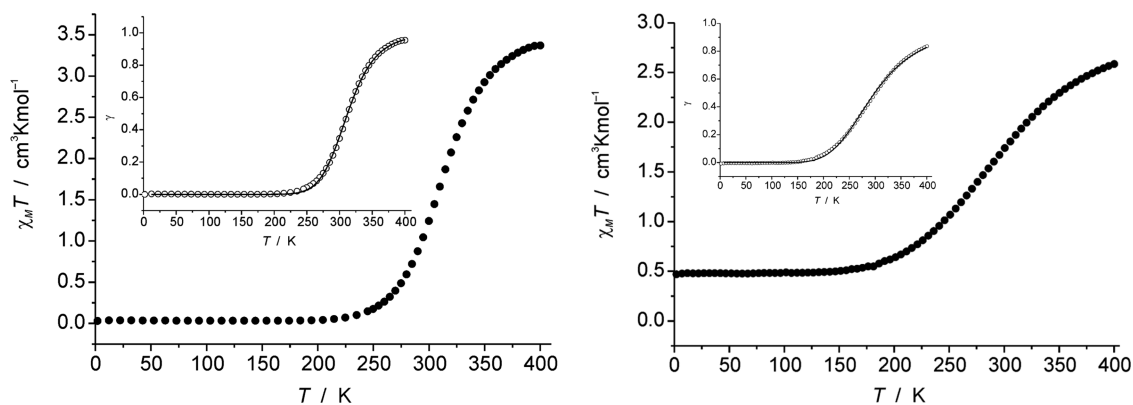
Figure 5. $\chi_M T$ vs T plot of **4** (left) and **6** (right), obtained from SQUID measurements at 5000 Oe. Insets show plots of the HS molar fraction (γ) vs temperature T; the solid lines represent the fit to the experimental data using the domain model with $n = 1$ (see text).

phenomenon is observed only for complex **4**, where the intramolecular C−H···π and other NCI exist (see the Discussion section on crystal structure, presented earlier in this paper). For complexes **1−3**, where these interactions are destroyed by the solvent molecules, the system remains locked in the HS state in the entire investigated temperature range. A similar behavior was observed in related complexes [Fe{(HC-$(3,5\text{-Me}_2\text{pz})_3\}_2$]I$_2$ (where pz is the pyrazolyl ring) and its solvate [Fe{(HC$(3,5\text{-Me}_2\text{pz})_3\}_2$]I$_2\cdot$4CH$_2Cl_2$.[3l,p] In those cases, the solvent-free complex shows SCO, whereas the solvated complex remains locked in the HS at all investigated temperatures. The difference in the spin states in those two complexes was correlated to torsion angles at the metal centers, as has been discussed in the structural section above. In the present case, complexes **1−3** have torsion angles at the Fe center that are largely different from those observed for **4**. The crystals of **4** measured at 293 K delivered torsion angles that are identical to those observed at 133 K. This is an indication that the torsion angles in the HS state of **4** is likely to be similar to those observed for its LS state. For **1−3**, the smaller torsion angles observed in the HS state forces those complexes to remain locked in that spin state as the large structural changes needed to reach the LS state cannot be compensated by changes in temperatures.

Attempts at generating **4** by heating samples of **1−3** to 400 K inside the SQUID magnetometer were not successful. Independent experiments showed that heating of **1−3** lead to a loss of crystallinity of these samples, and the resulting color of the heated solid did not match that of **4**. We have not been able to identify the fate of the sample generated by heating **1−3**; however, **4** was certainly not generated during that process.

The spin and oxidation state of the Fe complex **4** was further probed by Mössbauer spectroscopy (Figure 6). **4** shows an isomer shift of 0.56 mm s^{-1} at 80 K, indicating the exclusive existence of a LS Fe(II) center at that temperature, a result which is consistent with the information obtained from SQUID measurements.

The solvent-free Co(II) complex **6** shows a magnetic behavior that is identical to complex **5**, which was recently published by us.[8] Thus, the counterion does not seem to play any significant role in the magnetic properties of these complexes. The $\chi_M T$ vs T curve for **6** is shown in Figure 5 (right part). The value of 2.59 cm^3 mol^{-1} K observed at higher temperatures is consistent with a HS Co(II) center containing a $S = 3/2$ state. Upon cooling the sample, a change to the LS state is observed with a $T_{1/2}$ of ca. 300 K. Below 150 K, the
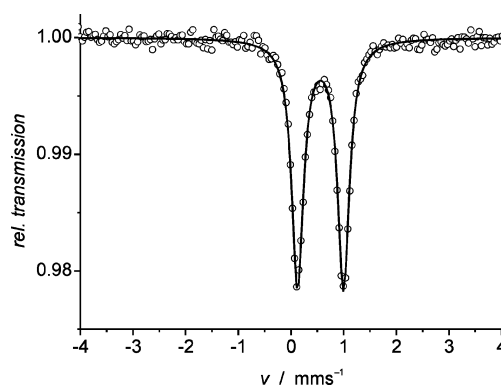

Figure 6. Mössbauer spectrum of **4** at 80 K.

complex shows a $\chi_M T$ value of 0.49 cm^3 mol^{-1} K, which is consistent with the existence of a LS ($S = 1/2$) Co(II) state. Thermodynamic parameters for the SCO in **6** are $\Delta H = 15.5$ kJ mol^{-1}, $\Delta S = 52$ J mol^{-1} K^{-1} (using the above model with domain size parameter $n = 1$); these values are similar to those determined earlier for complex **5** with different counteranions ($\Delta H = 13.9$ kJ mol^{-1}, $\Delta S = 43$ J mol^{-1} K^{-1}). Similar to Fe complex **4**, also in the case of **5** and **6**, ΔH and ΔS are appreciably higher than those usually found for Co-based SCO systems with more-rigid ligands.[5a,8] Thus, just like **4**, **6** shows a SCO behavior with a relative high $T_{1/2}$ value. The sum of the torsion angles at the metal centers, as discussed above, are similar for the solvent-free Fe(II) complex **4** and its analogous Co(II) complex **6**. The SCO and the high $T_{1/2}$ value for **6** are driven by NCIs and their effect on the torsion angles, as has been discussed previously for **4**. The spin state of the Co(II) complex was also probed by EPR spectroscopy. At 110 K in the solid state, **6** shows a signal that is typical for a LS Co(II) center (see Figure S5 in the Supporting Information). The spectrum could be simulated with the parameters $g_\perp = 2.220$, $g_\parallel = 2.020$, $A_\perp = 29.3$ G, and $A_\parallel = 75.7$ G. Because of the relatively narrow lines association with a $S = 1/2$ LS Co(II) center, the hyperfine coupling to the nuclear spin of Co(II) ($I = 7/2$) is also resolved.

Hence, it is seen that the same ligand environment is capable of producing thermal SCO for Fe(II) in **4** and for Co(II) in **5** and **6**. This observation is an extremely rare one, because usually a different ligand field is required for driving SCO in Co(II) complexes, compared to their Fe(II) counterparts. As a result, different types of ligands are usually required for
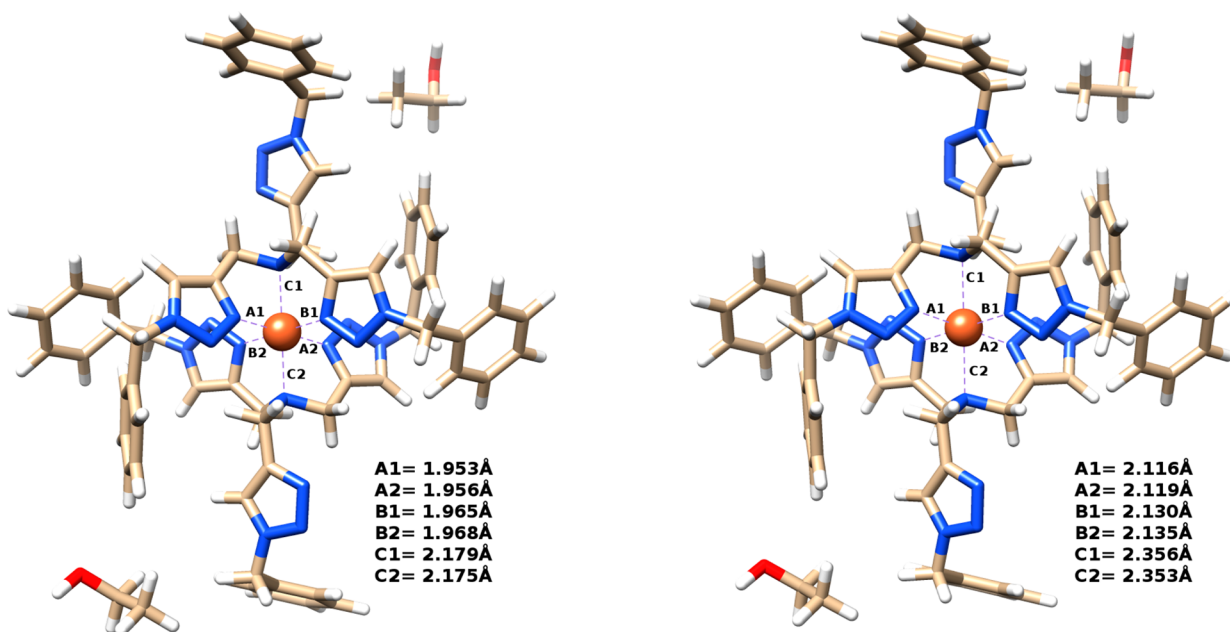
Figure 7. Optimized structures for each spin state of **1** on the PBE-D3/600 eV level, together with selected bond lengths ((left) low-spin (LS) state, (right) high spin (HS) state).
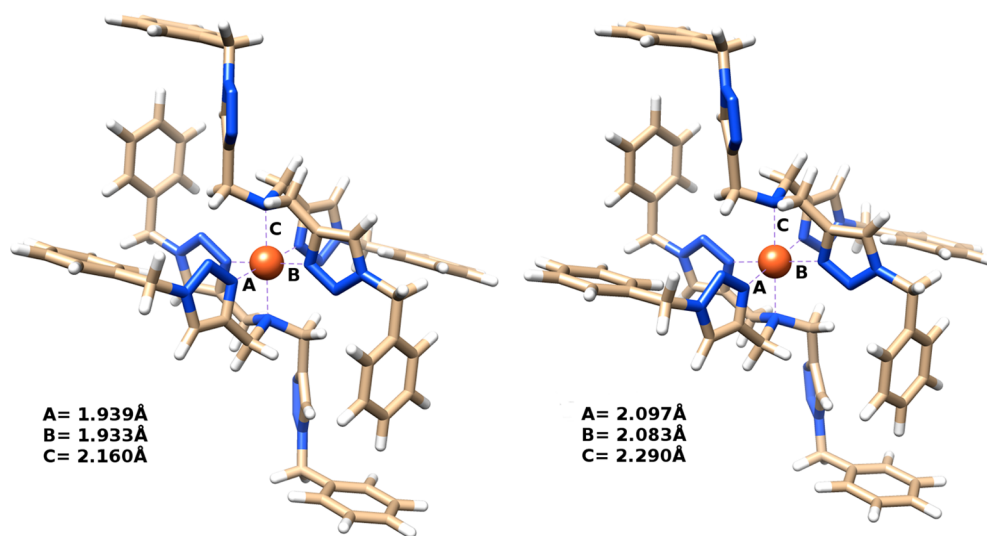
Figure 8. Optimized structures for each spin state of **4** on the PBE-D3/600 eV level, together with selected bond lengths ((left) low-spin (LS) state, (right) high spin (HS) state).

observing SCO in Fe(II) and Co(II) complexes. For example, whereas the complex [Fe{(HC(3,5-Me$_2$pz)$_3$}$_2$]I$_2$ mentioned above displays SCO, the Co(II) analogue with the same ligands remains HS at all the investigated temperatures. Hence, this is a rare example where identical ligand environments drive SCO in both Fe(II) and Co(II) complexes. We believe this phenomenon is related to the contribution of NCIs made possible through the benzyl substituents (see DFT section below) of the tbta ligand, and their effect on the torsion angles at the metal centers in SCO behavior.

DFT Calculations. In the following, we theoretically investigate the question if the energy of the LS state of the solvent-free complex **4** is lowered by noncovalent (C–H···π) interactions (NCI). Molecules **2** and **3** are not explicitly treated here, but the trends are similar to **1**, as shown in the Supporting Information.

First, we confirm the measured spin state of complex **1** and complex **4** by comparison with the corresponding calculated crystal structures in the HS state and LS state, respectively. The four structures (including counterions) are optimized in periodic boundary conditions on the PBE-D3/600 eV level[19] with the VASP 5.3 simulation package.[20] Long-range electron correlation effects are treated with the atom-pairwise London dispersion correction D3.[21] The optimized structures of complexes **1** and **4** are shown in Figures 7 and 8, respectively.

By comparing selected bond lengths with the experimental X-ray structure, we conclude that complex **1** is indeed in the HS state while complex **4** is in its LS state. Typical deviations between theory and experiment for the investigated bond lengths are small, which also verifies the accuracy of the theoretical equilibrium structure.

Second, we calculated the energy difference between HS and LS states to investigate the effect of the molecular stacking, i.e., the different NCI. Note that, for a straightforward comparison, one must regard each state in its optimized structure. Otherwise, a bias toward the experimentally observed spin state is introduced. These (biased) vertical excitations are presented, together with a diagnosis of the spin contamination, in the Supporting Information. In order to make the calculations affordable, we performed single-point calculations on the molecular geometries taken from the optimized crystal structures. We utilized several dispersion-corrected density functionals with a large Gaussian AO def2-TZVP basis set[22] using the TURBOMOLE 6.3 suite of programs.[23] At this level, basis set errors are negligible. The final relative energies for the HS−LS splitting (ΔE(HS-LS)) are presented in Table 2. The

Table 2. Energy Difference (ΔE(HS-LS)) for HS and LS States from Single-Point Calculations of the Molecular Structures without Counterions Based on the Optimized Crystals 1 and 4 for Various Density Functionals[a]

molecule	Energy Difference, ΔE(HS-LS) (kcal/mol)				
	PBE-D3 (periodic)	PBE-D3	TPSSh-D3	B3LYP-D3	PBE0-D3
1	15.9	17.3	7.0	−6.4	−11.6
4	25.7	24.1	13.6	0.7	−5.0
Δ(4−1)	9.8	6.8	6.6	7.1	6.6

[a]A positive value denotes a more-stable LS state.

(periodic) PBE-D3 calculations compute a stabilization of the LS state (from complex **1** to complex **4**) by 10 kcal/mol. This qualitatively agrees with the experiment and strongly indicates the significant impact of NCI on the spin state. The good agreement between the periodic PBE-D3/600 eV with the molecular PBE-D3/def2-TZVP results justifies the applied procedure. The slightly stronger LS stabilization in periodic boundaries even emphasizes the importance of NCI.

However, in absolute energies, the LS state is the minimum at the PBE-D3 level for both complexes. This is due to an artificial stabilization of the LS state by GGA density functionals such as PBE.[24] The performance of the density functional for this property can be improved by incorporating admixtures of Fock exchange (known as hybrid functionals). The energy splitting with three dispersion-corrected hybrid functionals with different amount of Fock exchange (TPSSh-D3: 10%,[25] B3LYP-D3: 20%,[26] PBE0-D3: 25%[27]) is presented in the second part of Table 2. The widely used B3LYP-D3 functional calculates an energy splitting in agreement with the experimental findings. However, one must note that the splitting is very sensitive to the amount of Fock exchange, e.g., on the PBE0-D3 level, both complexes are calculated to be in the HS state. This is a known problem of hybrid functionals applied to transition-metal complexes.[24] Therefore, we focus on the relative splitting, i.e., the (relative) stabilization of the LS state of complex **4**, in comparison to complex **1**. All tested (hybrid) density functionals give a comparable LS state lowering of the solvent-free compound **4**.

Although our theoretical investigation cannot predict the spin state in advance, we have (i) a theoretical model that reproduces the experimental observations (B3LYP-D3) and (ii) good evidence that the stacking of complex **4** with strong NCI stabilizes the LS state.

CONCLUSIONS

The "click"-derived ligand tris[(1-benzyl-1H-1,2,3-triazol-4-yl)methyl]amine (tbta) has been successfully utilized in generating spin crossover (SCO) complexes in this work. The substituents on the tbta ligand can be chosen to generate various noncovalent interactions (NCIs) in these metal complexes. These interactions influence the torsion angles at the metal centers and indirectly (by structural changes) influence the ligand field strength in the complexes and preferentially stabilize the LS state at lower temperatures. The same interactions and changes in torsion angles also help in driving the SCO process in these solvent-free metal complexes, as proved by the examples of Fe(II) and Co(II) compounds. The introduction of solvent molecules of a particular size and polarity destroys these NCIs in the secondary coordination sphere, changes the torsion angles at the metal centers, and locks the molecules in the high-spin (HS) state. Data obtained from single-crystal X-ray diffraction (XRD), SQUID magnetometry, EPR spectroscopy, and Mössbauer spectroscopy corroborate the observations and hypothesis. In addition, we have used density functional theory (DFT) calculations to get insights into the role of noncovalent interaction (NCI) in influencing the spin state of the metal complexes, and these calculations confirm the stabilization of the LS spin through NCIs. To the best of our knowledge, this is one of the rare occasions where such calculations have been performed to get insights into the role played by NCI in determining spin states of molecules. We have thus shown the applications of "click"-derived ligands in the field of magnetic bistability. In addition, we have modified these interactions by structural changes to influence the spin state of these molecules. Finally, we have used theoretical modeling to understand the correlation between NCI and the spin state of metal centers. This combined approach thus opens new avenues for "click" ligands in coordination chemistry and magnetically bistable systems. We have also presented a rare example of a case where the same ligand set can drive SCO in Fe(II) complexes as well as Co(II) complexes.

EXPERIMENTAL SECTION

Materials and General Methods. All the chemicals used in this work were used as received. The metal salts were purchased from ABCR (A Better Choice for Research), and all the chemicals required for the synthesis of tbta were purchased from Sigma−Aldrich. The solvents were purchased from VWR (Van Waters and Rogers) and used without further purification; tbta was synthesized according to a reported procedure.[28] Elemental analyses were performed with a Perkin−Elmer Analyzer 240 system. Electron paramagnetic resonance (EPR) spectra in the X-band were recorded with a Bruker EMX system.

Synthesis. [Fe(TBTA)₂](BF₄)₂·2EtOH (1). tbta (100 mg, 0.19 mmol) and Fe(BF₄)₂·6H₂O (31.8 mg, 0.09 mmol) were dissolved in ethanol (8 mL). The solution was refluxed for 1 h and allowed to cool. The precipitate was filtered off and the filtrate was collected. After the slow diffusion of diethyl ether on top of the filtrate, colorless single crystals suitable for X-ray diffraction (XRD) were collected. Anal. Calcd for $C_{64}H_{72}B_2F_8FeN_{20}O_2$: C, 55.59; H, 5.25; N, 20.26. Found: C, 55.57; H, 5.13; N, 20.29.

[Fe(TBTA)₂](BF₄)₂·2CH₃CN (2). tbta (100 mg, 0.19 mmol) and Fe(BF₄)₂·6H₂O (31.8 mg, 0.09 mmol) were dissolved in acetonitrile (5 mL). The solution was refluxed for 1 h and allowed to cool. The precipitate was filtered off and the filtrate was collected. After the addition of toluene (5 mL) to the filtrate, the solution was stored at 8 °C. Colorless single crystals suitable for X-ray diffraction could be

collected from the solution. Anal. Calcd for $C_{64}H_{66}B_2F_8FeN_{22}$: C, 55.99; H, 4.85; N, 22.45. Found: C, 56.05; H, 5.04; N, 22.18.

[Fe(TBTA)$_2$](BF$_4$)$_2$·2CHCl$_3$ (3). tbta (100 mg, 0.19 mmol) and Fe(BF$_4$)$_2$·6H$_2$O (31.8 mg, 0.09 mmol) were dissolved in ethanol (10 mL). The solution was refluxed for 1 h. The solvent then was evaporated and the remaining solid was dried under high vacuum. The dry substance was dissolved in chloroform (2 mL). After the slow diffusion of ether on top of the solution, colorless single crystals suitable for XRD were collected. Anal. Calcd for $C_{62}H_{62}B_2Cl_6F_8FeN_{20}$: C, 48.69; H, 4.09; N, 18.32. Found: C, 48.52; H, 3.74; N, 18.09.

[Fe(TBTA)$_2$](BF$_4$)$_2$ (4). tbta (100 mg, 0.19 mmol) and Fe(BF$_4$)$_2$· 6H$_2$O (31.8 mg, 0.09 mmol) were dissolved in propylene glycol (5 mL). The solution was refluxed for 1 h and allowed to cool. The precipitate was filtered off and the yellow filtrate was collected. After the slow diffusion of ether on top of the filtrate, yellow single crystals suitable for XRD were collected. Anal. Calcd for $C_{60}H_{60}B_2F_8FeN_{20}$: C, 55.83; H, 4.69; N, 21.70. Found: C, 55.76; H, 4.55; N, 21.61.

[Co(TBTA)$_2$](BF$_4$)$_2$ (6). tbta (100 mg, 0.19 mmol) and Co(BF$_4$)$_2$· 6H$_2$O (32.4 mg, 0.09 mmol) were dissolved in methanol (8 mL). The solution was refluxed for 1 h. The solution then was allowed to cool slowly. From this solution, pink single crystals suitable for XRD were collected the next day. Anal. Calcd for $C_{60}H_{60}B_2CoF_8N_{20}$: C, 55.70; H, 4.67; N, 21.65. Found: C, 55.10; H, 4.41; N, 21.39.

X-ray Crystallography. The intensity data were collected at 100(2) K upon a using a Bruker Kappa Apex II duo diffractometer or at 133(2) K on a Stoe IPDS II. Crystallographic and experimental details for the structures are summarized in Table S1 in the Supporting Information. The structures were solved by direct methods (SHELXS-97) and refined by full-matrix least-squares procedures (based on F^2, SHELXL-97 or SHELXL-2013).[29] SADI restraints (d_{B-F}, $d_{F\cdots F}$) were applied to model the disorder of the BF$_4^-$ in **1** (occupancy factors of 0.586(9)/0.414(9)). Atoms of the dangling phenyl group in **1** show some higher displacement parameters, in comparison to the other atoms of the molecule. This is not unusual and treatment as a disorder would only lead to more restraints and constraints with only minor (if at all) improvements of the overall quality of the structure determination. Since checkcif gave only C level alerts (except for the "D-H without acceptor" alert for the calculated hydrogen atom position of the solvent O−H), we decided to publish this structure without refinement of a disorder of this part. CCDC Nos. 804869 and 911107−911110 contain the supplementary crystallographic data for this paper. These data can be obtained free of charge from The Cambridge Crystallographic Data Centre (www.ccdc.cam.ac.uk/data_request/cif).

Magnetic Susceptibility Measurements. Temperature-dependent magnetic susceptibility measurements were carried out with a Quantum Design Model MPMS-XL-5 SQUID magnetometer that was equipped with a 5 T magnet in the range from 295 K to 2.0 K at a magnetic field of 0.5 T. The powdered sample was contained in a gel bucket and fixed in a nonmagnetic sample holder. Each raw data file for the measured magnetic moment was corrected for the diamagnetic contribution of the gel bucket, according to M^{dia}(gel bucket) = $\chi_g mH$, with an experimentally obtained gram susceptibility of the gel bucket $\chi_g = -4.7 \times 10^{-7}$ emu/(g Oe). The molar susceptibility data were corrected for the diamagnetic contribution, according to χ_M^{dia}(sample) = $-0.5M \times 10^{-6}$ cm^3 mol^{-1}.[30a] Magnetic susceptibility χ was used as gram susceptibility (χ_g) for diamagnetic correction of sample holder, and as molar susceptibility (χ_M) for diamagnetic correction of sample itself. Moreover, note that 1 emu/Oe = 1 cm^3; other symbols have their usual meaning (m, mass; M, molar weight; H, magnetic field strength).

For verification of this method, the diamagnetic correction of **1** was also implemented using the Pascal constants and the increment method according to Haberditzl.[31] Values obtained from both methods differ by 0.03%−1.2%, depending on the temperature, which is within the limits of the accuracy of the measurement.

The HS molar fraction γ was calculated according to

$$\gamma = \frac{\chi T - (\chi T)_{LS}}{(\chi T)_{HS} - (\chi T)_{LS}}$$

Thermodynamic parameters of the SCO transition were calculated according to the domain model:

$$\gamma = \frac{1}{1 + \exp(n\cdot\Delta H/RT - n\cdot\Delta S/R)}$$

where ΔH and ΔS are the enthalpy and entropy parameters, R is the universal gas constant, and n is the domain size and represents the number of molecules per domain.[30] The fit of the magnetic data were performed by use of the program Origin 6.1 from OriginLab Corporation.

Mössbauer Spectroscopy. The Mössbauer spectra were recorded with a ^{57}Co source in a Rh matrix using an alternating constant acceleration Wissel Mössbauer spectrometer operated in the transmission mode and equipped with a Janis closed-cycle helium cryostat. The isomer shift is given relative to iron metal at ambient temperature. Simulation of the experimental data was performed with the Mfit program using Lorentzian line doublets (E. Bill, Max-Planck Institute for Chemical Energy Conversion, Mülheim/Ruhr, Germany. E-mail: eckhard.bill@cec.mpg.de; webpage: http://www.cec.mpg.de/research/molecular-theory-and-spectroscopy/moessbauer-mcd.html?L=1).

Theoretical Studies. All molecular calculations were carried out with the TURBOMOLE 6.3 program package.[23] The initial structures are based on X-ray data without any counteranions, and the bonds containing a hydrogen atom were set to 1.089 Å (C−H bond) and 0.950 Å (O−H bond). For the vertical excitations molecular single-point calculations were performed on these structures. We utilized the meta-GGA TPSS and the corresponding meta-hybrid TPSSh,[25] together with the Ahlrichs' type triple-ζ basis set def2-TZVP.[22] We expect that the noncovalent interactions in the structures, as found in the crystal, indirectly influence the electronic structure and, hence, the state splitting. Therefore, free molecular structure optimizations that are normally performed in quantum chemical calculations are not applied, because they would lead to structures that are significantly different from those of the solid state. We used the resolution of identity (RI-J) approximation.[32] To simulate bulk solvent effects, COSMO[33] was employed in all calculations with a dielectric constant of $\varepsilon = \infty$. In order to check for broken symmetry solutions, the low-spin (LS) states were recalculated unrestricted by starting with converged high-spin (HS) state orbitals. The results of these calculations were denoted by the code "BS" (for broken symmetry). For systems **1** and **4**, we optimized the crystal geometries with periodic boundary conditions. These calculations were carried out with the Vienna Ab-initio Simulation Package (VASP).[20] Thereby, we utilized the GGA functional PBE[19] in the combination with a projector-augmented plane wave basis set (PAW)[34] with an energy cutoff of 600 eV and sampled the Brillouin zone at the Γ-point. The molecular crystals were optimized with fixed unit cells. For the optimization of the atomic coordinates, we used an extended version of the approximate normal coordinate rational function optimization program (ANCOPT)[35] until all forces are below 10^{-4} a.u. We also included the D3 dispersion energy in the Becke−Johnson damping scheme and a conservative distance cutoff of 100 a.u.[21] In addition, single-point calculations on the same level as previously described were carried out with three different GGAs—namely, TPSS, BLYP and PBE[19,24,25]—and the corresponding hybrid functionals TPSSh, B3LYP, and PBE0,[25−27] which differ also by the admixture of Fock exchange (10%, 20%, and 25%, respectively) besides the different exchange and correlation parts. Here, the D3 correction using the Becke−Johnson damping scheme applied as well.[21,35]

■ ASSOCIATED CONTENT

⑤ Supporting Information

CIF files and tables giving the crystallographic details for **1**−**4** and **6**; ORTEP plots of **2**, **3**, and **4**; $\chi_M T$ vs T plots of **1**−**3**; EPR spectrum of **6**; DFT tables; discussion on vertical excitations and spin contamination; and CIF files of the optimized BE-D3/600 eV structures for the LS and HS state of

1 and **4**. This material is available free of charge via the Internet at http://pubs.acs.org.

■ AUTHOR INFORMATION

Corresponding Authors
*E-mail: grimme@thch.uni-bonn.de (S. Grimme).
*E-mail: Biprajit.sarkar@fu-berlin.de (B. Sarkar).

Notes
The authors declare no competing financial interest.

■ REFERENCES

(1) Gispert, J. R. *Coordination Chemistry*; Wiley−VCH: Weinheim, Germany, 2008.

(2) (a) *Spin Crossover in Transition Metal Compounds I−III*; Gütlich, P., Goodwin, H. A., Eds.; Topics in Current Chemistry, Vols. 233−235; Springer: Berlin, Heidelberg, Germany, 2004. (b) *Magnetism: A Supramolecular Function*; NATO ASI Series C484; Kahn, O., Ed.; Kluwer Academic Publishers: Dordrecht, The Netherlands, 1996; pp 335−356. (c) *Eur. J. Inorg. Chem.* 2013, 574−1067 (Cluster Issue on Spin Crossover Complexes).

(3) For selected reviews and examples, see: (a) Real, J. A.; Gaspar, A. B.; Munoz, M. C. *Dalton Trans.* 2005, 2062. (b) Sato, O.; Tao, J.; Zhang, Y.-Z. *Angew. Chem., Int. Ed.* 2007, 46, 2152. (c) Gamez, P.; Costa, J. S.; Quesada, M.; Aromi, G. *Dalton Trans.* 2009, 7845. (d) Salitros, I.; Madhu, N. T.; Boca, R.; Pavlik, J.; Ruben, M. *Monatsch. Chem.* 2009, 140, 695. (e) Tao, J.; Wei, R.-J.; Huang, R.-B.; Zheng, L.-S. *Chem. Soc. Rev.* 2012, 41, 703. (f) Halcrow, M. A. *Chem. Soc. Rev.* 2011, 40, 4119. (g) Schneider, B.; Demeshko, S.; Dechert, S.; Meyer, F. *Angew. Chem.* 2010, 122, 9461. (h) Ikuta, Y.; Ooidemizu, M.; Yamahata, Y.; Yamada, M.; Osa, S.; Matsumoto, N.; Iijima, S.; Sunatsuki, Y.; Kojima, M.; Dahan, F.; Tuchagues, J.-P. *Inorg. Chem.* 2003, 42, 7001. (i) Arata, S.; Torigoe, H.; Iihoshi, T.; Matsumoto, N.; Dahan, F.; Tuchagues, J.-P. *Inorg. Chem.* 2005, 44, 9288. (j) Collet, E.; Watanabe, H.; Bréfuel, N.; Palatinus, L.; Roudaut, L.; Toupet, L.; Tanaka, K.; Tuchagues, J.-P.; Fertey, P.; Ravy, S.; Toudic, B.; Cailleau, H. *Phys. Rev. Lett.* 2012, 109, 257206. (k) Lemercier, G.; Bréfuel, N.; Shova, S.; Wolny, J. A.; Dahan, F.; Verelst, M.; Paulsen, H.; Trautwein, A. X.; Tuchagues, J.-P. *Chem.—Eur. J.* 2006, 12, 7421. (l) Reger, D. L.; Little, C. A.; Smith, M. D.; Rheingold, A. L.; Lam, K.-C.; Concolino, T. L.; Long, G. J.; Hermann, R. P.; Grandjean, F. *Eur. J. Inorg. Chem.* 2002, 1190. (m) Reger, D. L.; Little, C. A.; Rheingold, A. L.; Lam, M.; Concolino, T.; Mohan, A.; Long, G. J. *Inorg. Chem.* 2000, 39, 4674. (n) Leger, D. L.; Little, C. A.; Rheingold, A. L.; Lam, M.; Liable-Sands, L. M.; Rhagitan, B.; Concolino, T.; Mohan, A.; Long, G. J.; Briois, V. *Inorg. Chem.* 2001, 40, 1508. (o) Leger, D. L.; Little, C. A.; Young, V. G., Jr.; Pink, M. *Inorg. Chem.* 2001, 40, 2870. (p) Long, G. J.; Grandjean, F.; Reger, D. L. *Top. Curr. Chem.* 2004, 233, 91.

(4) For selected reviews and examples, see: (a) Bronisz, R. *Inorg. Chem.* 2007, 46, 6733. (b) Shongwe, M. S.; Al-Rashdi, B. A.; Adams, H.; Morris, M. J.; Mikuriya, M.; Hearne, G. R. *Inorg. Chem.* 2007, 46, 9558. (c) Brefuek, N.; Watanabe, H.; Toupet, L.; Come, J.; Matsumoto, N.; Collet, E.; Tanaka, K.; Tuchagues, J. P. *Angew. Chem., Int. Ed.* 2009, 48, 9304. (d) König, E.; Ritter, G.; Kulshreshthat, S. K. *Chem. Rev.* 1985, 85, 219. (e) Gütlich, P.; Hauser, A.; Spiering, H. *Angew. Chem., Int. Ed.* 1994, 33, 2024. (f) Gütlich, P.; Garcia, Y.; Goodwin, H. A. *Chem. Soc. Rev.* 2000, 29, 419.

(5) For selected examples and reviews, see: (a) Goodwin, H. A. *Top. Curr. Chem.* 2004, 234, 23. (b) Krivokapic, I.; Zerara, M.; Daku, M. L.; Vargas, A.; Enachesu, C.; Ambrus, C.; Pigot, P. T.; Amstutz, N.; Krausz, E.; Hauser, A. *Coord. Chem. Rev.* 2007, 251, 364. (c) Hayami, S.; Urakami, D.; Kojima, Y.; Yoshizaki, H.; Yamamoto, Y.; Kato, K.; Fuyuhiro, A.; Kawata, S.; Inoue, K. *Inorg. Chem.* 2010, 49, 1428. (d) Brooker, S.; Plieger, P. G.; Moubaraki, B.; Murray, K. S. *Angew. Chem., Int. Ed.* 1999, 38, 408. (e) Beckmann, U.; Brooker, S. *Coord. Chem. Rev.* 2003, 245, 17. (f) Brooker, S. *Eur. J. Inorg. Chem.* 2002, 2535. (g) Murray, K. S. *Eur. J. Inorg. Chem.* 2008, 3101.

(6) (a) Kahn, O.; Martinez, C. J. *Science* 1998, 279, 44. (b) Matsuda, M.; Isokazi, H.; Tajima, H. *Chem. Lett.* 2008, 37. (c) Müller, R. N.; van der Elst, L.; Laurent, S. *J. Am. Chem. Soc.* 2003, 125, 8405. (d) Kröber, J.; Codjovi, E.; Kahn, O.; Grolière, F.; Jay, C. *J. Am. Chem. Soc.* 1993, 115, 9819.

(7) (a) Weber, B.; Bauer, W.; Obel, J. *Angew. Chem., Int. Ed.* 2008, 47, 10098. (b) Bhattacharjee, A.; Ksenofontov, V.; Sugiyarto, K. H.; Goodwin, H. A.; Gütlich, P. *Adv. Funct. Mater.* 2003, 13, 877. (c) Bréfuel, N.; Imatomi, S.; Torigoe, H.; Hagiwara, H.; Shova, S.; Meunier, J.-F.; Bonhommeau, S.; Tuchagues, J.-P.; Matsumoto, N. *Inorg. Chem.* 2006, 45, 8126. (d) Buchen, T.; Gütlich, P.; Sugiyarto, K. H.; Goodwin, H. A. *Chem.—Eur. J.* 1996, 2, 1134. (e) Summerton, A. P.; Diamantis, A. A.; Snow, M. R. *Inorg. Chim. Acta* 1978, 27, 123. (f) Weber, B.; Bauer, W.; Pfaffeneder, T.; Dirtu, M. M.; Naik, A. D.; Rotaru, A.; Garcia, Y. *Eur. J. Inorg. Chem.* 2011, 3193. (g) Phan, H. V.; Charaborty, P.; Chen, M.; Calm, Y. M.; Kovnir, K.; Keniley, L. K., Jr.; Hoyt, J. M.; Knowles, E. S.; Besnard, C.; Meisel, M. W.; Hauser, A.; Achim, C.; Shatruk, S. *Chem.—Eur. J.* 2012, 18, 15805.

(8) Schweinfurth, D.; Weisser, F.; Bubrin, D.; Bogani, L.; Sarkar, B. *Inorg. Chem.* 2011, 50, 6114.

(9) (a) Liang, L.; Astruc, D. *Coord. Chem. Rev.* 2011, 255, 2933. (b) Struthers, H.; Mindt, T. L.; Schibli, R. *Dalton Trans.* 2010, 39, 675. (c) Crowley, J. D.; McMorran, D. In *Topics in Heterocyclic Chemistry*, Vol. 22; Kosmrlj, J., Ed.; Springer: Berlin, Heidelberg, Germany, 2012; p 31. (d) Schweinfurth, D.; Deibel, N.; Weisser, F.; Sarkar, B. *Nachr. Chem.* 2011, 59, 937. (e) Aromi, G.; Barrios, L. A.; Roubeau, O.; Gamez, P. *Coord. Chem. Rev.* 2011, 255, 485.

(10) For selected examples, see: (a) Li, Y.; Huffman, J. C.; Flood, A. H. *Chem. Commun.* 2007, 2692. (b) Ostermeier, M.; Berlin, M.-A.; Meudtner, R. M.; Demeshko, S.; Meyer, F.; Limberg, C.; Hecht, S. *Chem.—Eur. J.* 2010, 16, 10202. (c) Yang, W. W.; Wang, L.; Zhong, Y. W.; Yao, Y. *Organometallics* 2011, 30, 2236. (d) Swanick, K. N.; Ladouceur, S.; Zysman-Colman, E.; Ding, Z. *Chem. Commun.* 2012, 48, 3179. (e) Brown, D. G.; Sanguantrakun, N.; Schulz, B.; Schubert, U. S.; Berlinguette, C. P. *J. Am. Chem. Soc.* 2012, 134, 12354. (f) Guha, P. M.; Phan, H.; Kinyon, J. S.; Brotherton, W. S.; Sreenath, K.; Simmons, J. T.; Wang, Z.; Clark, R. J.; Dalal, N. S.; Shatruk, M.; Zhu, L. *Inorg. Chem.* 2012, 51, 3465. (g) Crowley, J. D.; Bandeen, P. H. *Dalton Trans.* 2010, 39, 612. (h) Urankar, D.; Pevec, A.; Kosmrlj, J. *Cryst. Growth Des.* 2010, 10, 4920. (i) Clough, M. C.; Zeits, P. D.; Bhuvanesh, N.; Gladysz, J. A. *Organometallics* 2012, 31, 5231. (j) Stevenson, K. A.; Melan, C. F. C.; Fleischel, O.; Wang, R.; Petitjean, A. *Cryst. Growth Des.* 2012, 12, 5169. (k) Maisonial, A.; Serafin, P.; Traikia, M.; Debiton, E.; Théry, V.; Eitken, D. J.; Lemoine, P.; Viossat, B.; Gautier, A. *Eur. J. Inorg. Chem.* 2008, 298. (l) Ségaud, N.; Rebilly, J.-N.; Sénéchal-David, K.; Guillot, R.; Billon, L.; Baltaze, J.-P.; Farjon, J.; Reinaud, O.; Banse, F. *Inorg. Chem.* 2013, 52, 691. (m) Anderson, C. B.; Elliot, A. B. S.; Lewis, J. E. M.; McAdam, C. J.; Gordon, K. C.; Crowley, J. D. *Dalton Trans.* 2012, 41, 14625. (n) Oton, F.; Gonzalez, M. D. C.; Espinosa, A.; Táragga, A.; Molina, P. *Organometallics* 2012, 31, 2085.

(11) (a) Schweinfurth, D.; Pattacini, R.; Strobel, S.; Sarkar, B. *Dalton Trans.* 2009, 9291. (b) Schweinfurth, D.; Strobel, S.; Sarkar, B. *Inorg. Chim. Acta* 2011, 374, 253. (c) Hohloch, S.; Su, C.-Y.; Sarkar, B. *Eur. J. Inorg. Chem.* 2011, 3067. (d) Schweinfurth, D.; Demeshko, S.; Khusniyarov, M. M.; Dechert, S.; Gurram, V.; Buchmeiser, M. R.; Meyer, F.; Sarkar, B. *Inorg. Chem.* 2012, 51, 7592. (e) Schweinfurth, D.; Su, C.-Y.; Wei, S.-C.; Braunstein, P.; Sarkar, B. *Dalton Trans.* 2012, 41, 12984. (f) Schweinfurth, D.; Krzystek, J.; Schapiro, I.; Demeshko, S.; Klein, J.; Telser, J.; Ozarowski, A.; Su, C.-Y.; Meyer, F.; Atanasov, M.; Neese, F.; Sarkar, B. *Inorg. Chem.* 2013, 52, 6880. (g) Schweinfurth, D.; Klein, J.; Hohloch, S.; Dechert, S.; Demeshko, S.; Meyer, F.; Sarkar, B. *Dalton Trans.* 2013, 42, 6944. (h) Schweinfurth, D.; Büttner,

N.; Hohloch, S.; Deibel, N.; Klein, J.; Sarkar, B. *Organometallics* **2013**, *32*, 5834.

(12) (a) Nihei, M.; Han, L.; Oshio, H. *J. Am. Chem. Soc.* **2007**, *129*, 5312. (b) Reger, D. L.; Little, C. A.; Smith, M. D.; Rheingold, A. L.; Lam, K.-C.; Concolino, T. L.; Long, G. R.; Hermann, R. P.; Grandjean, F. *Eur. J. Inorg. Chem.* **2002**, 1190.

(13) (a) McCusker, J. K.; Rheingold, A. L.; Hendrickson, D. N. *Inorg. Chem.* **1996**, *35*, 2100. (b) Guionneau, P.; Machivie, M.; Bravic, G.; Létard, J.-F.; Chasseau, D. *Top. Curr. Chem.* **2004**, *234*, 97.

(14) Hua, Y.; Flood, A. H. *Chem. Soc. Rev.* **2010**, *39*, 1262.

(15) (a) Sorai, M.; Seki, S. *J. Phys. Chem. Solids* **1974**, *35*, 555. (b) Kahn, O. *Molecular Magnetism*; VCH Publishers: New York, 1993.

(16) Berezovskii, G. A.; Lavrenova, L. G. *J. Therm. Anal. Calorim.* **2011**, *103*, 1063.

(17) ΔS values are often much larger than the entropy gain expected from the change in the spin multiplicity (13.4 J mol^{-1} K^{-1}), indicating a significant phonon contribution.

(18) Boča, R. *Solid State Phenom.* **2003**, *90−91*, 141.

(19) (a) Perdew, J. P.; Burke, K.; Ernzerhof, M. *Phys. Rev. Lett.* **1996**, *77*, 3865. (b) Perdew, J. P.; Burke, K.; Ernzerhof, M. *Phys. Rev. Lett.* **1997**, *78*, 1396.

(20) (a) Kresse, G.; Furthmüller, J. *Comput. Mater. Sci.* **1996**, *6*, 15. (b) Bucko, T.; Hafner, J.; Lebegue, S.; Angyan, J. G. *J. Phys. Chem. A* **2010**, *114*, 11814.

(21) (a) Grimme, S.; Antony, J.; Ehrlich, S.; Krieg, H. *J. Chem. Phys.* **2010**, *132*, 154104. (b) Grimme, S.; Ehrlich, S.; Goerigk, L. *J. Comput. Chem.* **2011**, *32*, 1456.

(22) Weigend, F.; Ahlrichs, R. *Phys. Chem. Chem. Phys.* **2005**, *7*, 3297.

(23) TURBOMOLE V6.3 2011, a development of University of Karlsruhe and Forschungs-zentrum Karlsruhe GmbH, 1989−2007, TURBOMOLE GmbH, since 2007.

(24) (a) Zein, S.; Borshch, S. A.; Fleurat-Lessard, P.; Casida, M. E.; Chermette, H. *J. Chem. Phys.* **2007**, *126*, 014105. (b) Vancoillie, S.; Zhao, H.; Radoń, M.; Pierloot, K. *J. Chem. Theory Comput.* **2010**, *6*, 576. (c) Swart, M. *J. Chem. Theory Comput.* **2008**, *4*, 2057. (d) Swart, M.; Groenhof, A. R.; Ehlers, A. W.; Lammertsma, K. *J. Phys. Chem. A* **2004**, *108*, 5479. (e) Swart, M. *Inorg. Chim. Acta* **2007**, *360*, 179. (f) Reiher, M.; Salomon, O.; Hess, B. A. *Theor. Chem. Acc.* **2001**, *107*, 48. (g) Salomon, O.; Reiher, M.; Hess, B. A. *J. Chem. Phys.* **2002**, *117*, 4729.

(25) Tao, J. M.; Perdew, J. P.; Staroverov, V. N.; Scuseria, G. E. *Phys. Rev. Lett.* **2003**, *91*, 146401.

(26) (a) Becke, A. D. *Phys. Rev. A* **1988**, *38*, 3098. (b) Lee, C.; Yang, W.; Parr, R. G. *Phys. Rev. B* **1988**, *37*, 785. (c) Becke, A. D. *J. Chem. Phys.* **1993**, *98*, 5648.

(27) Ernzerhof, M.; Scuseria, G. E. *J. Chem. Phys.* **1999**, *110*, 5029.

(28) Hein, J. E.; Krasnova, L. B.; Iwasaki, M.; Fokin, V. V. *Org. Synth.* **2011**, *88*, 238.

(29) Sheldrick, G. M. *Acta Crystallogr., Sect. A: Found. Crystallogr.* **2008**, *A64*, 112.

(30) (a) Kahn, O. *Molecular Magnetism*; VCH Publishers: New York, 1993. (b) Sorai, M.; Seki, S. *J. Phys. Chem. Solids* **1974**, *35*, 555.

(31) (a) Haberditzel, W. *Angew. Chem., Int. Ed. Engl.* **1966**, *5*, 288. (b) Bain, G. A.; Berry, J. F. *J. Chem. Educ.* **2008**, *85*, 532.

(32) Vahtras, O.; Almlöf, J.; Feyereisen, M. W. *Chem. Phys. Lett.* **1993**, *213*, 514.

(33) Klamt, A.; Schüürmann, G. *J. Chem. Soc., Perkin Trans. 2* **1993**, 795.

(34) (a) Blöchl, P. E. *Phys. Rev. B* **1994**, *50*, 17953. (b) Kresse, G.; Joubert, D. *Phys. Rev. B* **1999**, *59*, 1758.

(35) Grimme, S. *ANCOPT: Approximate normal coordinate rational function optimization program*, University of Bonn: Bonn, Germany, 2013.